Turkish Journal of Electrical Engineering & Computer Sciences

http://journals.tubitak.gov.tr/elektrik/

Research Article

Turk J Elec Eng & Comp Sci
(2020) 28: 432 – 442

doi:10.3906/elk-1804-141

RMS frequency error performance and spurious signals in two-point modulators due to path imbalances

Gökhun SELÇUK*, Kaan ÜÇEL
Electronics Design Department, Communication and Information Technologies Business Sector, ASELSAN Inc., Ankara, Turkey

Received: 19.04.2018 • **Accepted/Published Online:** 11.09.2019 • **Final Version:** 27.01.2020

Abstract: In this study the authors introduce an analysis of rms frequency error performance and spurious signals generated by two-point modulators. The analysis is not limited to a constant delay and magnitude imbalance between modulation paths but allows frequency-dependent group delay and amplitude variations as well. Moreover, a discrete time phase frequency detector model is incorporated in Laplace domain analysis that takes into account the sampling nature of a phase-locked loop (PLL). Using the spectrum of pulse width modulated charge pump pulses, the spurious signals at the output of the PLL are evaluated. The proposed formulae are tested on a practical setup and quite accurate results are obtained.

Key words: Frequency error, phase-locked loop, pulse width modulation, two-point modulator

1. Introduction

Two-point modulators are effective means of generating analogue/digitally modulated signals with wide modulation bandwidths. These modulators can be used to generate constant envelope signals with no additional circuit elements or they can be used along with envelope modulators at successive stages to generate polar transmitters for nonconstant envelope modulation [1]. Since the modulation is achieved within a phase-locked loop (PLL) and no external elements are required for modulation, modulators with low power demand and high integrity can be implemented with relatively low cost. The modulating signal is applied both to the reference signal, which exhibits a low pass response, and to the voltage controlled oscillator (VCO), which exhibits a high pass response. This circumvents the bandwidth problem and provides uniform modulation sensitivity unless there exists imbalance between modulation paths. The imbalance between the modulating paths introduces two major distortions into the signal: i) due to imbalance, the modulation sensitivity is not uniform and rms frequency error is increased, ii) since the VCO and reference are not in phase at the input of the phase detector (PD), the charge pump is activated, producing unwanted spurious signals at the output of the VCO.

Given the modulation-coding scheme of the communication network, the requirement on the rms frequency error of a transmitter is determined according to the tolerable throughput loss [2]. In general, total distortion of a transmitter is dominated by the nonlinearity of the power amplifier. Therefore, distortion due to transmit filters, phase noise of VCO, and modulators should have little influence on total distortion. This requires careful treatment of different contributors and detailed analysis is mandatory at the design stage.

*Correspondence: gselcuk@aselsan.com.tr

Other imperfections, namely spurious emissions, should also be estimated accurately to allow a high number of users within the limited frequency band. Unwanted signals at the output of the two-point modulator can be a major contributor to unwanted emissions, which deserve special attention. In the present study these two shortcomings of two-point modulators are addressed. Although frequency error is the major performance criterion of a two-point modulator, most studies dealing with two-point modulators do not present any detailed analysis but only introduce final results [3, 4]. In [5] a rigorous analysis of EVM for Gaussian frequency shift keying (GFSK) signals is introduced but it is valid only for constant delay and constant amplitude mismatch. Moreover, it is not clear how the method should be modified to account for M-ary modulating signals. On the other hand, the practical modulation paths have a frequency response and this should be taken into account for accurate predictions. Furthermore, constant envelope M-ary modulation formats are desirable to obtain higher throughput with efficient power amplifiers. Another performance parameter of two-point modulators, namely the spurious signals, cannot be analyzed using the conventional s-domain analysis since this method misses the sampling nature of PLL. Spurious signals generated by PLLs are investigated in the time domain in [6], but this method is applicable only to amplitude imbalance and single tone modulating signals. A sampling model for the phase frequency detector (PFD) is introduced in [7], which also accounts for spurious signals. However, the appearance of spurious signals is neglected as they are filtered by loop components and no expression about the level of these signals at the output of the PLL is introduced. Despite the fact that this approach leads to correct results as far as band signals are concerned, due to the strict spectrum mask requirements of today's communication systems the filtering of the loop may not be adequate and analysis of these signals is essential. In the present study, using the spectrum of pulse width modulated (PWM) pulses from [8], the author replaces the conventional PFD model with a new model to account for pulses generated at the output of the charge pump. The proposed methods are tested on a practical setup and coherent results with the measurements are obtained.

2. Two-point modulator analysis

The block diagram of a PLL used to generate constant envelope phase/frequency modulated signals is shown in Figure 1. The transmit data, with Fourier transform $M(j\omega)$, are fed both to the VCO, whose tuning sensitivity is $K_{VCO}/(j\omega)$, and to the reference signal, whose tuning sensitivity is $K_{REF}/(j\omega)$. At the high frequency portion of the TX data signal (beyond the loop bandwidth) the VCO modulation path is dominant and at the low frequency portion of the TX data the reference oscillator modulation is dominant.

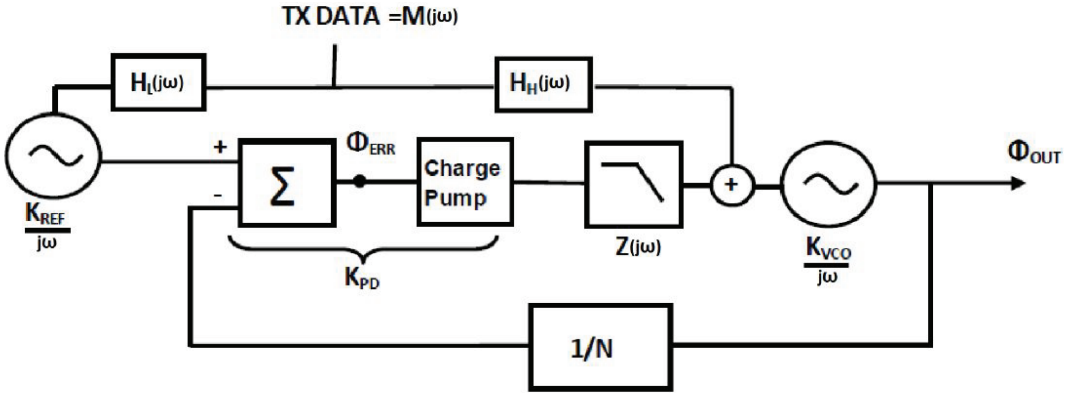

Figure 1. Two-point modulator block diagram using a fractional-N synthesizer.

The phase of the reference oscillator is compared with the phase of the VCO after being divided by N at the phase frequency detector and an error signal is generated according to the difference between phases. The charge pump produces up/down pulses whose duration is determined by the magnitude of phase difference between pulses. Here the combined response of the PFD and the charge pump is denoted by $K_{PFD} = I_{cp}/2\pi$ for frequency domain analysis. These pulses are smoothed at the loop filter, whose frequency domain response is $Z(j\omega)$, to modulate the VCO.

The two filters with responses $H_L(j\omega)$ and $H_H(j\omega)$ in Figure 1 account for the amplitude and phase distortions of the low frequency and high frequency paths, respectively. When only the reference oscillator path is used to generate modulation, the output phase $\Theta_{OUT,REF}(j\omega)$ is written as

$$\Theta_{OUT,REF}(j\omega) = M(j\omega)H_L(j\omega)\frac{K_{REF}N}{j\omega}\left[\frac{A(j\omega)}{1+A(j\omega)}\right], \tag{1}$$

where $A(j\omega)$ is the open loop transfer function with

$$A(j\omega) = K_{PFD}Z(j\omega)\frac{K_{VCO}}{j\omega}\frac{1}{N} \tag{2}$$

In a similar way, when only the VCO path is used to generate modulation, the output phase $\Theta_{OUT,VCO}(j\omega)$ is written as

$$\Theta_{OUT,VCO}(j\omega) = M(j\omega)H_H(j\omega)\frac{K_{VCO}}{j\omega}\left[\frac{1}{1+A(j\omega)}\right] \tag{3}$$

When the modulating signal is not subject to any distortion at modulation paths such that $H_L(j\omega) = H_H(j\omega) = 1$ and if the condition $K_{VCO} = NK_{REF}$ is satisfied, then superposition of Equation 2 and Equation 3 leads to a perfect FM modulator with tuning sensitivity K_{VCO}.

2.1. Frequency error due to path imbalances

In practical implementations the modulation paths do not possess a uniform transmission characteristic. First of all, the VCO is an analogue component and the tuning port is designed using analogue components that introduce a frequency response to the port. Moreover, if an integer-N synthesizer is employed, imperfect modulation characteristics of the reference oscillator introduce distortion. The output response is obtained by summing Equation 1 and Equation 3. Without loss of generality we can assume that $K_{VCO} = NK_{REF}$ since any mismatch can be included in the responses of $H_L(j\omega)$ or $H_H(j\omega)$. Thus the output phase is written as

$$\Theta_{OUT}(j\omega) = M(j\omega)\frac{K_{VCO}}{j\omega}\left[\frac{A(j\omega)H_L(j\omega) + H_H(j\omega)}{1+A(j\omega)}\right] \tag{4}$$

The response in the brackets on the RHS of Equation 4 is denoted by $H_{Total}(j\omega)$ and is the reason for rms frequency error. At the output of an FM demodulator with response $j\omega/K_{VCO}$, the recovered signal is written as

$$\hat{M}(j\omega) = M(j\omega)\left[\frac{A(j\omega)K_L(j\omega) + H_H(j\omega)}{1+A(j\omega)}\right] = M(j\omega)H_{Total}(j\omega) \tag{5}$$

It is clear from Equation 5 that the level of error of the signal $M(j\omega)$ can be analyzed using the characteristics of the filter $H_{Total}(j\omega)$. Here the EVM calculation from [9] is borrowed to evaluate the error caused by amplitude and phase fluctuations of $H_{Total}(j\omega)$. According to Equation 9, the EVM of the signal in Equation 5 can be evaluated using

$$EVM \approxeq \sqrt{(\Delta Amp_{rms})^2 + \tan(\Delta Phs_{rms})^2}, \tag{6}$$

where ΔAmp_{rms} is the rms amplitude fluctuation and ΔPhs_{rms} is the rms phase fluctuation, given by

$$\Delta Amp_{rms} = \sqrt{\frac{1}{2W}\int_{-W}^{W}\left[\frac{\mid H_{Total}(j\omega) \mid - H_{Total,rms}}{H_{Total,rms}}\right]^2 df} \tag{7}$$

$$\Delta Phs_{rms} = \sqrt{\frac{1}{2W}\int_{-W}^{W}\left[\angle H_{Total}(j\omega) - \angle H_{Total,rms}\right]^2 df}, \tag{8}$$

where $H_{Total,rms}$ is the rms value of the filter amplitude response and $\angle H_{Total,rms}$ is the linearized phase and W is the bandwidth of the baseband signal. Using the filter analogy to evaluate the distortion of the baseband signal has two advantages. Firstly, it is easily applicable to M-ary modulation schemes and it is not required to evaluate the average frequency deviation for each level of signaling. Secondly, rather than evaluating distortion on the RF bandwidth, as is the case in [5], it is adequate to evaluate distortion within the bandwidth of the baseband signal, which can be far narrower depending on the application.

Use of $H_{Total,rms}$ and $\angle H_{Total,rms}$ does not lead to correct results when measurements are obtained using conventional vector signal analyzers. This is because in estimation of the deviation error and frequency error of a signal the vector signal analyzer makes a joint estimation for which these errors are treated separately and the frequency error is evaluated after the contribution of deviation error is subtracted [10]. Here $H_{Total,rms}$ is replaced by $H_{Total,opt}$ and $\angle H_{Total,rms}$ is replaced by $\angle H_{Total,opt}$ to obtain coherent results with the measurement device. Thus

$$H_{Total,opt} = arg\ min_{H_{Total,rms}}(\Delta A_{rms}) \tag{9}$$

$$\angle H_{Total,opt} = arg\ min_{\angle H_{Total,rms}}(\Delta P_{rms}) \tag{10}$$

2.2. Spurious signals generated by PLL

Another distortion mechanism introduced due to imbalance between modulation paths is the spurious signals generated at the charge pump frequency and at its harmonics. The PFD output is a series of pulses whose widths are determined by the difference between the phases of the reference clock and divided VCO. The pulses repeat themselves at $T_{REF} = 1/f_{REF}$ and the spectrum of the pulse train consists of a baseband term plus the harmonic terms separated by f_{REF}. Given the time domain phase error at the output of PFD $\Theta_{err}(t)$, the pulses at the output of the charge pump are plotted in Figure 2.

It is obvious that due to sampling operation the replica of the $I_{cp}(f)$ is produced at integer multiples of sampling frequency f_{REF}. In order to determine the magnitude of the replicas, [7] uses a heuristic approach by replacing the pulse width modulated (PWM) pulses with impulses whose magnitude is determined by the width of the pulses. Using this approach all replicas of I_{cp} have the same magnitude and shape but are scaled

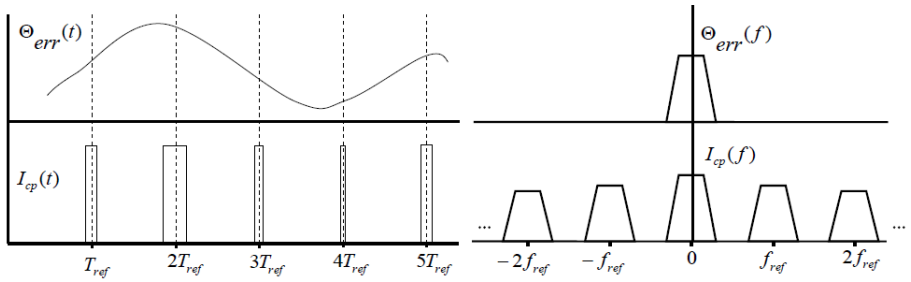

Figure 2. The phase error and related charge pump: time-domain signals and frequency domain representation.

by $1/T_{REF}$. This approach is valid when the duty cycle of the pulse train is small, but there is no analytical criterion for this assumption and the resulting error.

When the duty cycle is not small, the spectrum of the PWM signal contains harmonics of the modulating signal around the sampling frequency f_{REF}. When the input is represented by $\Theta_{err}(t)$, the three-state PWM output can be obtained by subtracting a square wave from a naturally sampled PWM with spectrum as [8]

$$PWM(f) = \Theta_{err}(f) + \sum_{k=1}^{\infty}(-1)^k \sum_{n=1}^{\infty} \frac{(jk\pi)^{n-1}}{n!}\Big\{S_n(f + kf_{REF}) + (-1)^{n-1}S_n(f - kf_{REF})\Big\}, \tag{11}$$

where S_n denotes the Fourier transform of $\Theta_{err}^n(t)$.

Equation 11 consists of infinitely many terms located around the harmonics of the reference frequency kf_{REF}. Obviously for small $\Theta_{err}(t)$ the term with $n = 1$ is dominant and the spectrum reduces to that introduced in [7]. When this is not the case the terms arising from the Fourier transform of $m^n(t)$ (n^{th} power of $m(t)$) become nonnegligible and have two distortive effects on the spectrum. Firstly, they contribute to the total power of the unwanted harmonics around kf_{REF}. Secondly, since they are Fourier transforms of $m^n(t)$, their spectrum is wider than that of $m(t)$ and are scaled by n. This may result in aliasing of the signal even if the bandwidth of the signals is less than $f_{REF}/2$. From the block diagram given in Figure 1, the phase difference with the input of the phase detector is given by

$$\Theta_{err}(j\omega) = M(j\omega)\left[\frac{K_{REF}\left[H_L(j\omega) - H_H(j\omega)\right]}{K_{PFD}K_{VCO}Z(j\omega) + N(j\omega)}\right] \tag{12}$$

The phase at the output of the VCO can be found by inserting Equation 11 into Equation 12 and then multiplying the resulting spectrum by the responses of the loop filter and the VCO. This leads to

$$\Theta_{OUT}(j\omega) = \Theta_{PWM}(j\omega)K_{PFD}Z(jm\omega_{REF})\frac{K_{VCO}}{jm\omega_{REF}} \tag{13}$$

Since the loop has a low pass response, the terms at the harmonics of the phase detector are drastically attenuated. Therefore, narrow band frequency modulation (FM) can be used to estimate the level of the spurious signal as [11]

$$A_{spur} = 20\log\left[\Theta_{OUT}(j\omega)\right] \quad (dBc) \tag{14}$$

3. Results

The proposed formulae are tested on a practical setup by comparing measured results for spurious signals and the frequency error with the simulation results obtained by using the proposed formulae. For that purpose a

PLL with PD frequency of 25 MHz and an output frequency of 800 MHz is used, which results in a divide ratio of $N = 32$. The tuning sensitivity of the reference is adjusted to $K_{REF} = 625\ kHz/V$ and the tuning sensitivity of the VCO is $K_{REF} = 20\ MHz/V$. The charge pump current of the PFD is adjusted to $I_{cp} = 5.4\ mA$. A third order passive loop filter, whose elements are given in Figure 3, is used to smooth the charge pump pulses.

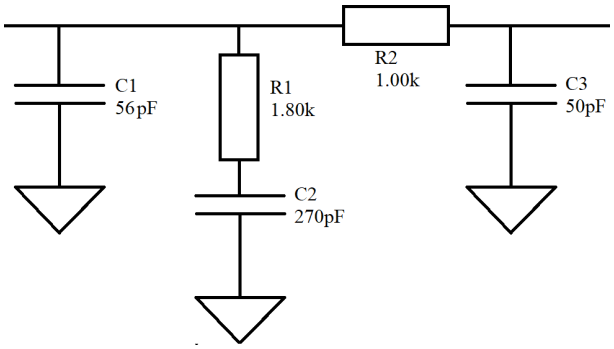

Figure 3. Topology and component parameters of the loop filter used in the PLL.

The above-mentioned parameters, along with $H_L(j\omega) = H_H(j\omega) = 1$, lead to a PLL whose closed loop bandwidth is around 700 kHz. Using Equation 1, Equation 3, and Equation 5, the modulation response of the VCO path, reference path, and combined response is plotted in Figure 4.

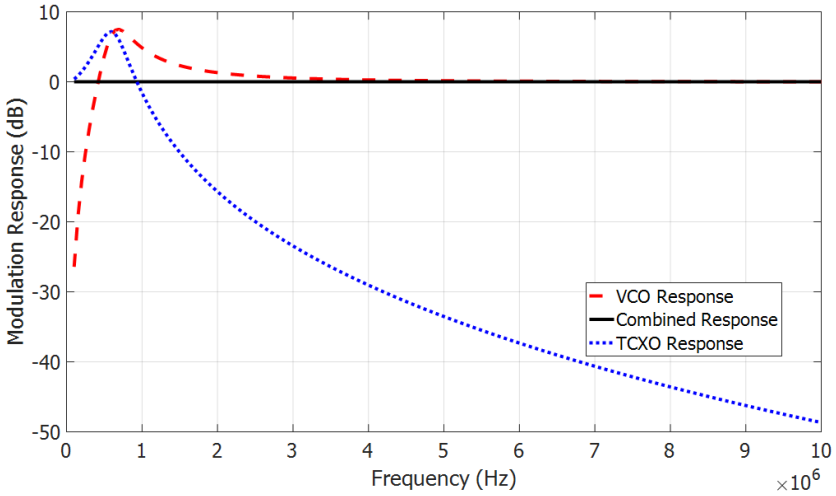

Figure 4. Modulation responses of the VCO and reference used in the PLL.

A 4-level frequency shift keying (4FSK) signal with rate 5 Mb/s that is filtered by an RRC filter of $\alpha = 0.5$ is applied to the PLL. In order to test the FSK_{err}, a filter with 3 dB corner frequency of 6 MHz is used as the distortion filter. Figure 5 shows the amplitude and group delay of the filter.

As the first step the frequency shift keying (FSK) error without the distortion filter is measured. This includes FSK error due to phase noise of the oscillator and imperfect modulation responses of the VCO and reference. The rms frequency error is measured around 3% and is recorded as $FSK_{err,floor}$. The resulting eye diagram is plotted in Figure 6.

Next the distortion filter is inserted either into the VCO modulation port or into the reference modulation port or into both ports. When the filter is inserted into a single port the group delay and attenuation of the other port are adjusted to obtain the lowest FSK error. Equation 7 and Equation 8 are used to calculate the

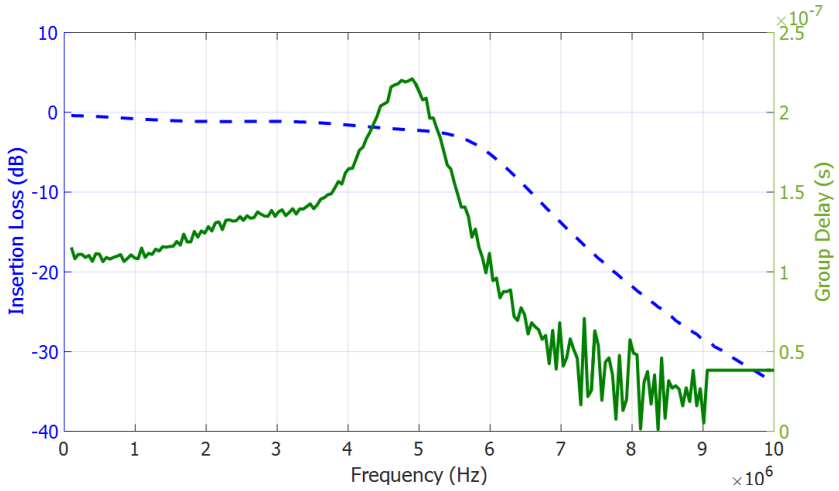

Figure 5. Amplitude and group delay response of the distortion filter.

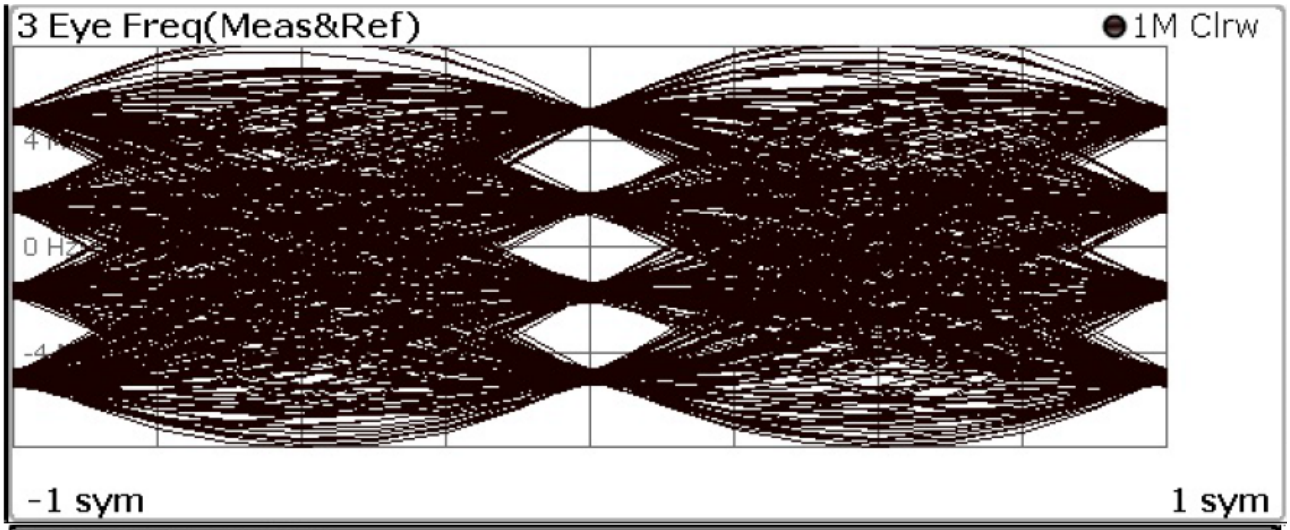

2 Result Summary

	Current	Peak	Unit
Frequency Error RMS	**2.99**	3.04	%
Peak	**-9.52**	-9.94	%
Magnitude Error RMS	**0.45**	0.46	%
Peak	**1.98**	2.70	%
FSK Deviation Error	**-98281.50**	-99975.50	Hz
FSK Meas Deviation	**4901718**	4906636	Hz
FSK Ref Deviation	**5000000**	5000000	Hz
Carrier Frequency Error	**44080.90**	62762.88	Hz
Carrier Frequency Drift	**-32.14**	70.03	Hz/sym
Power	**-2.82**	-2.81	dBm

Figure 6. Eye diagram of the two-point modulator without a distortion filter.

FSK error. The modulation response when the filter is in the reference port is plotted in Figure 7. This is

obtained by setting the attenuation of the VCO path to 0.65 dB and the group delay to 0.11 μs.

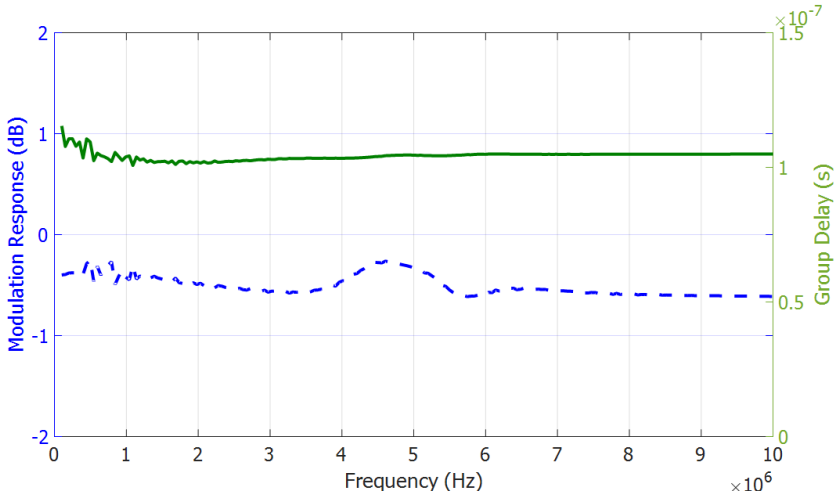

Figure 7. Combined modulation response when the distortion filter is on the reference path.

In each case measurements are obtained at 3 Msps and 5 Msps data rates and recorded. The total FSK error due to the distortion filter is evaluated using

$$FSK_{err,total} = \sqrt{FSK^2_{err,filter} + FSK^2_{err,floor}} \tag{15}$$

The measured results and the calculated results are given in Table 1.

Table 1. Comparison of simulated results with measurements (RMS frequency error).

	Data Rate	Freq. rms Error (Measured %)	Freq. rms Error (This Study %)
Dist. Filter on both paths	3 Msps	4.9	4.5
	5 Msps	15.4	13.9
Dist. Filter on reference path	3 Msps	3.9	3.6
	5 Msps	4.2	3.8
Dist. Filter on VCO path	3 Msps	4.6	4.3
	5 Msps	14.7	12.85

The results in Table 1 can be interpreted as follows: when the filter is in the reference port, the low-frequency portion up to loop bandwidth (up to 700 kHz) introduces error. For the VCO port the high-frequency portion (700 kHz to ∼1.5 MHz or ∼2.5 MHz) introduces error, which is larger due to the wider frequency range. When a filter is in both ports, the signal from DC to ∼1.5 MHz or ∼2.5 MHz introduces error, which is the largest. It can be observed from Table 1 that the measured results are coherent with the calculated ones. In Figure 8 the eye diagram is plotted for a 5 Msps signal and with the distortion filter on the VCO path.

In order to observe spurious signals at the output of the VCO, the same setup is used. When the distortion filter is inserted into both ports no spurious signals are observed since Θ_{err} in Equation 12 is zero. When the distortion filter is on the reference path, spurious signals are observed at the PD frequency. In order to boost the level of spurious signals no signal is applied to the VCO path. The imbalance transfer function of the loop, as given in Equation 12, is plotted in Figure 9. The figure also includes the spectrum of the data signal $M(j\omega)$ for a 3 Mb/s signal.

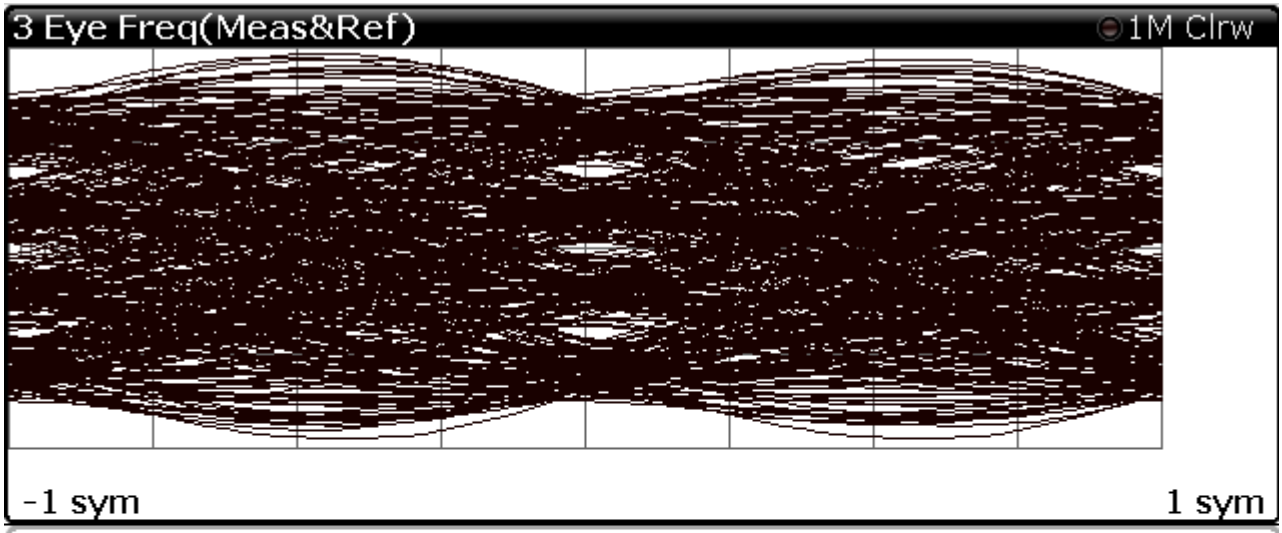

2 Result Summary

		Current	Peak	Unit
Frequency Error	RMS	**14.73**	30.75	%
	Peak	**47.41**	140.73	%
Magnitude Error	RMS	**0.87**	0.99	%
	Peak	**-3.55**	4.81	%
FSK Deviation Error		**-423742.00**	-1122515.50	Hz
FSK Meas Deviation		**4576258**	5726144	Hz
FSK Ref Deviation		**5000000**	5000000	Hz
Carrier Frequency Error		**81074.88**	2871357.00	Hz
Carrier Frequency Drift		**-74.36**	-2105.27	Hz/sym
Power		**-3.01**	-2.89	dBm

Figure 8. Eye diagram of the two-point modulator with a distortion filter on the VCO path.

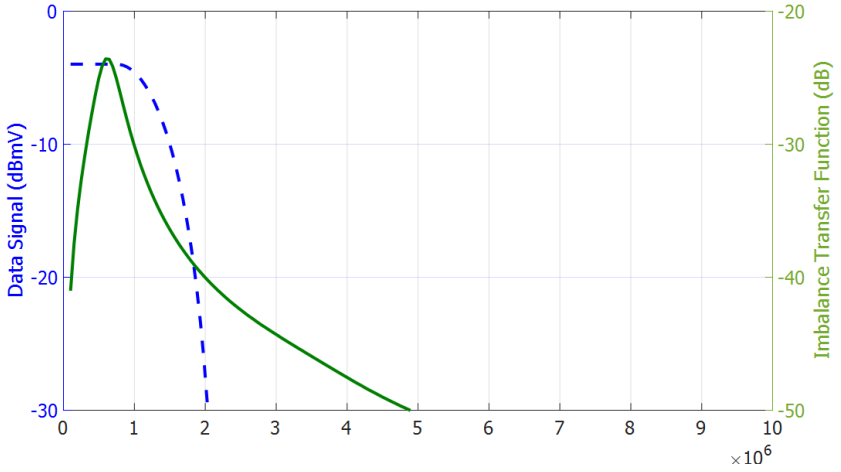

Figure 9. The imbalance transfer function and the spectrum of the data signal.

The power density at the spurious signal at $f = f_{REF}$ and $f = 2f_{REF}$ is evaluated using Equation 13, where the loop filter impedance is evaluated using the component values given in Figure 3. The total power within the channel bandwidth around the spurious signals is calculated as -41.8 dBc and -58.1 dBc, respectively.

In Figure 10 the VCO spectrum is plotted. The modulation signal widens the spectrum at the center frequency and this spectrum is translated to multiples of f_{REF}, whose amplitude is determined by integrating the spectrum in Equation 13 within channel bandwidth. The spurious signals are measured as -44.6 dBc and -60.1 dBc, respectively, the error between calculations and measurements being less than 3 dB.

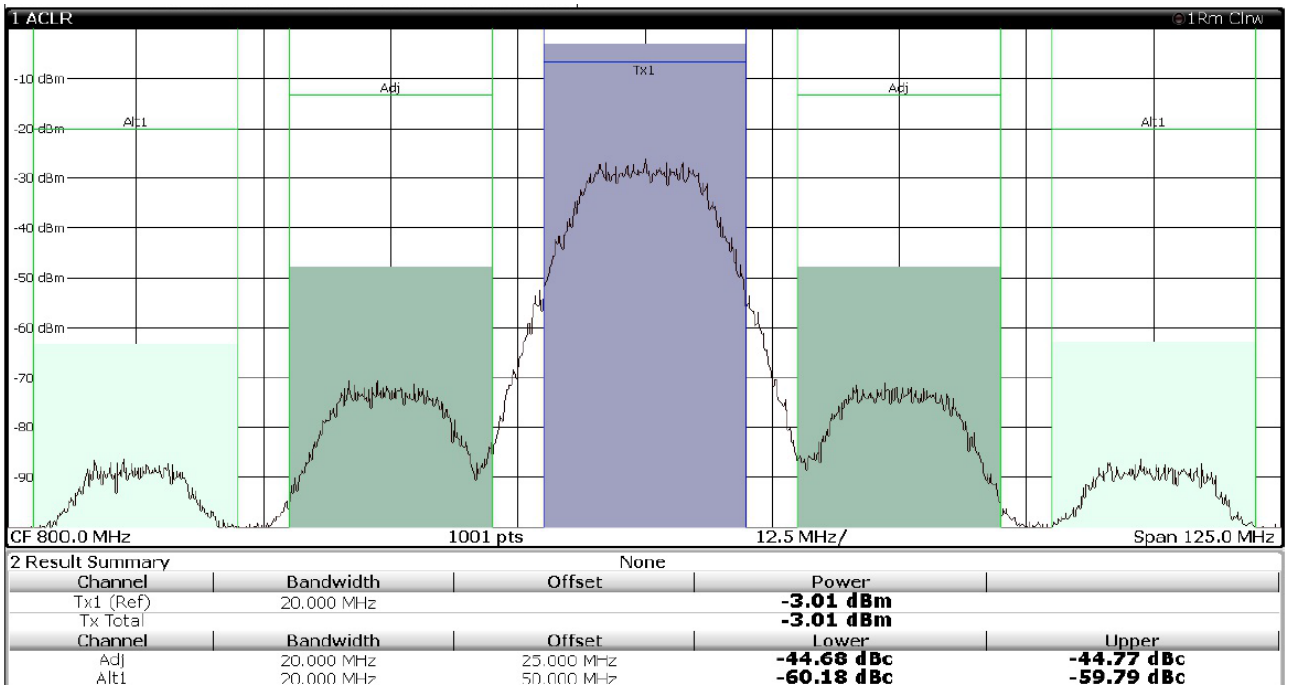

Figure 10. Spurious signals at the output of the VCO due to imbalance between modulation paths.

4. Conclusion

An analysis of rms frequency error performance and spurious signals for two-point modulators is introduced. Using a filter analogy for modulation error, the analysis is not limited to a constant delay and magnitude imbalance between modulation paths. Furthermore, the discrete time PFD model allows evaluation of the spurious signals generated by the PLL. The validity of the method is shown on a practical setup, where coherence is obtained between simulation results and practical measurements.

References

[1] Larrson L, Asbeck P, Kimball D. Multifunctional RF transmitters for next generation wireless transceivers. In: Proc IEEE Int Symp Circuits and Systems (ISCAS), 2007. pp. 753-756.

[2] Holma H, Toskala A. LTE for UMTS-OFDMA and SC_FDMA Based Radio Access. Chicester, UK: John Wiley and Sons, 2009.

[3] Lee S, Lee J, Park H, Lee KY, Nam S. Self-calibrated two-point delta-sigma modulation technique for RF transmitters. IEEE T Microw Theory Tech 2010; 58 (7): 1748-1757.

[4] Yu SA, Kinget P. A 0.65-V 2.5-GHz fractional-N synthesizer with two-point 2-Mb/s GFSK data modulation. IEEE J Solid-Stat Circ 2009; 44 (9): 2411-2425.

[5] Peng KC, Huang CH, Li CJ, Horng TZ. High-performance frequency-hopping transmitters using two-point delta-sigma modulation. IEEE T Microw Theory Tech 2004; 52 (11): 2529-2535.

[6] Selcuk G. Analysis of adjacent channel ratio performance in two-point modulated systems. In: Proc IEEE Sys Infor Modell Simul (SIMS), Riga, Latvia, 2016.

[7] Perrott MH, Trott MD, Sodini CG. A modeling approach for $\Sigma\Delta$ fractional-N frequency synthesizers allowing straightforward noise analysis. IEEE J Solid-Stat Circ 2002; 37 (8): 1028-1038.

[8] Pascual C, Song Z, Krein PT, Sarwate DV, Midya P, Roeckener WJ. High-fidelity PWM inverter for digital audio amplification: spectral analysis, real-time DSP implementation, and results. IEEE T Pow Elect 2003; 18 (1): 473-485.

[9] Pimingsdorfer D, Holm A, Adler B, Fisherauer G, Thomas R, Springer A, Weigel R. Impact of SAW RF and IF characteristics on UMTS transceiver system performance. In: Proc IEEE Int Syp Ultrasonics; Caesars Tahoe, NV, USA; 1999. pp.365-368.

[10] Rohde & Schwarz. R&S FSW-K70 Vector Signal Analysis User Manual. Munich, Germany: Rohde & Schwarz Company, 2014.

[11] Cicero A. Architectures for RF Frequency Synthesizers. New York, NY, USA: Kluwer, 2003.